PREDICTIVE ENGINEERING &
PECOS
COMPUTATIONAL SCIENCE

HYPERSONIC FLOW ON AN AXISYMMETRIC CAPSULE USING DPLR

James Strand
With assistance from Paul Bauman and Anthony West, and advised by David Goldstein
Predictive Engineering and Computational Science

Nomenclature

- Primitive variables:
  - ρ_i = species density
  - $\mathbf{u}$ = velocity vector
  - E_T = specific translational internal energy
  - E_v = specific vibrational energy
- Variables in constitutive relations:
  - ρ = density
  - p = pressure
  - $E = e + \mathbf{u}\cdot\mathbf{u}/2$ = total specific energy of the system (specific = per unit mass)
  - e = specific internal energy of the system
  - τ = viscous stress tensor
  - $\dot{\mathbf{q}}$ = heat flux vector (conduction, radiation, etc.)
  - T = translational temperature
  - T_v = vibrational temperature
  - e_{vs} = species specific vibrational energy
  - h_i = species enthalpy
  - c_s = species mass fraction
  - $\mu(T)$ = viscosity
  - $K_{eq}(T)$ = equilibrium constant
  - $k_{f/b}$ = forward/backward rate constant
  - θ_{vs} = species characteristic vibrational temperature
  - $\mathcal{D}_s$ = species s effective binary diffusivity
  - κ = thermal conductivity
- Parameters:
  - R = universal gas constant
  - k_B = Boltzmann's constant
  - m_s = species molecular weight
  - η, C_f, θ_d: Arrhenius parameters
  - C, A_1, A_2, A_3, A_4, A_5: Constants for K_{eq} curve fit

Governing Equations for Compressible Reacting Flows

$$\frac{\partial \rho_i}{\partial t} + \nabla\cdot(\rho_i\mathbf{u}) + \nabla\cdot(\rho\mathcal{D}_i\nabla c_i) = w_i$$
$$\frac{\partial(\rho\mathbf{u})}{\partial t} + \nabla\cdot(\rho\mathbf{u}\otimes\mathbf{u} + p\mathbf{I}) - \nabla\cdot\tau = 0$$
$$\frac{\partial(\rho E)}{\partial t} + \nabla\cdot(\rho E\mathbf{u} + p\mathbf{u} + \mathbf{q}) - \nabla\cdot(\tau\mathbf{u}) = 0$$
$$\frac{\partial(\rho E_v)}{\partial t} + \nabla\cdot\left(\rho E_v\mathbf{u} + \mathbf{q}_v + \sum_s^{\text{(diatomic)}} \rho_s e_{vs}\mathbf{u}_s\right) = w_v$$

where

$$\mathbf{q} = \underbrace{-\kappa\nabla T}_{\text{conduction}} + \underbrace{\sum_i \rho\mathcal{D}_i\nabla c_i h_i}_{\text{energy flux due to diffusion}} + \underbrace{\mathbf{q}_v}_{\text{vibration}} + \underbrace{\mathbf{q}_R}_{\text{radiation}}$$
$$\mathbf{q}_v = -\kappa_v\nabla T_v$$
$$e_{vs} = \frac{R\theta_s/m_s}{e^{\theta_s/T_v} - 1}$$

Note that μ and k are the *mixture* quantities.

Reacting flow:

$$\mathcal{R} = k_f\prod_j^r n_{R_j}^{\nu_j^{(r)}} - k_b\prod_j^p n_{P_j}^{\nu_j^{(p)}} \qquad \left(\sum_{i=1}^r \nu_i^{(r)}R_i \underset{k_b}{\overset{k_f}{\rightleftharpoons}} \sum_{i=1}^p \nu_i^{(p)}P_i\right)$$
$$w_s = m_s\sum_{\alpha=1}^{N_s^r}\dot{n}_\alpha$$
$$\dot{n}_{X_i} = \mathcal{R}\cdot\left[\nu_i^{(p)} - \nu_i^{(r)}\right]$$
$$T_a = T^q T_v^{1-q}$$
$$k_f(T_a) = C_f T_a^\eta \exp\left(\theta_d/T_a\right)$$
$$k_b(T_a) = \frac{k_f(T_a)}{K_{eq}(T)}$$
$$K_{eq}(T) = C\exp\left(A_1 + A_2 Z + A_3 Z^2 + A_4 Z^3 + A_5 Z^4\right) \qquad (Z = 10^4/T)$$

Parallel Efficiency

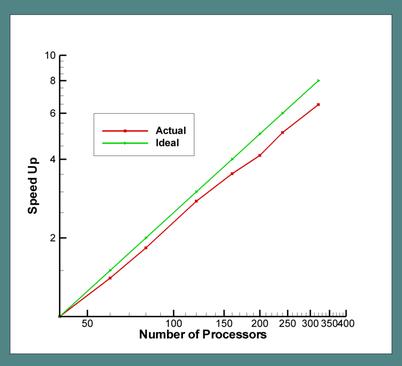

Plot of speedup vs. number of processors for full 3D CEV simulation, at 10 km/s and 157 degree angle of attack, with 11 species air. The 40 processor case is taken as the baseline. Load balancing is the same for all cases. Speedup for X processors is defined as the runtime with X processors divided by the runtime with 40 processors.

Grid Adaptation

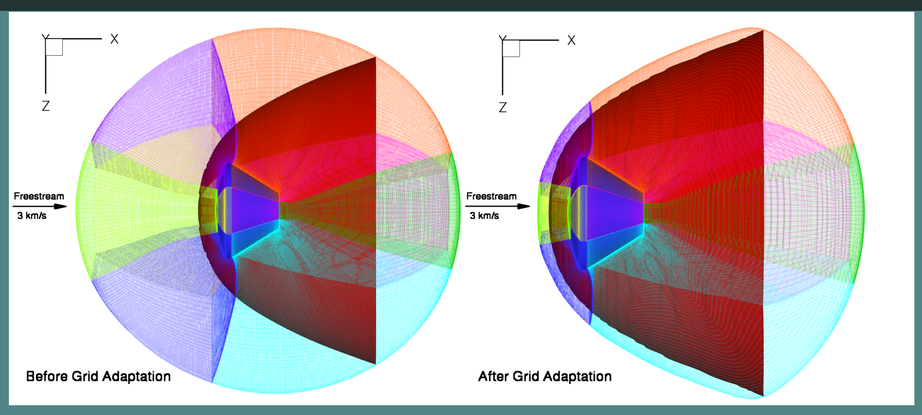

Comparison of unadapted and adapted NASA CEV grids for perfect gas simulation at 180 degree angle of attack. All 8 of the grid blocks can be seen (with each having a different mesh color in the images). The solid blue surface shows the location of the CEV and the solid red surface shows the location of the bow shock. The grid adaptation compresses the grid so that it extends just beyond the bow shock (while maintaining the same number of grid points), and thus greatly increases the grid resolution in the region of the bow shock.

Real Gas Effects

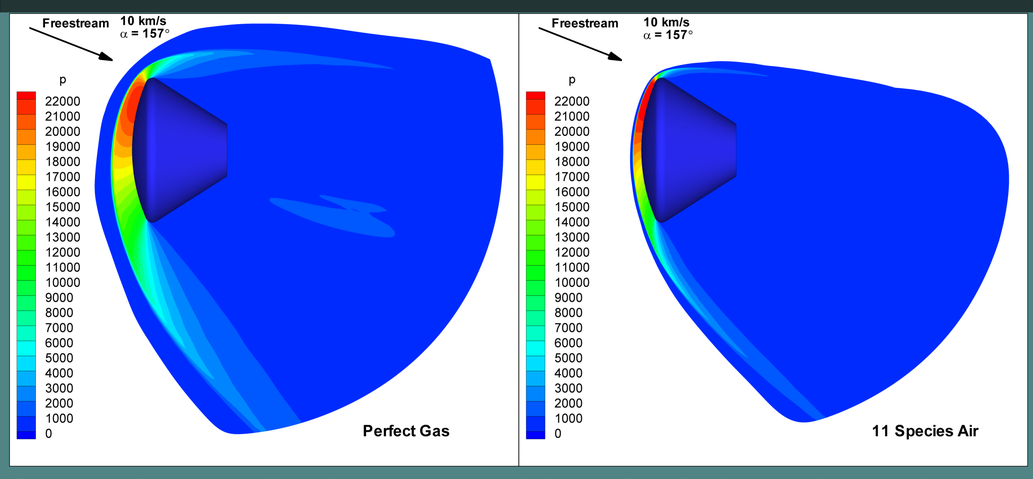

Contours of pressure. Note that the bow shock is significantly closer to the capsule in the 11 species case. However, the peak pressures and the overall pressure distributions are otherwise quite similar, since pressure is a mechanical quantity and is thus largely unaffected by flow chemistry.

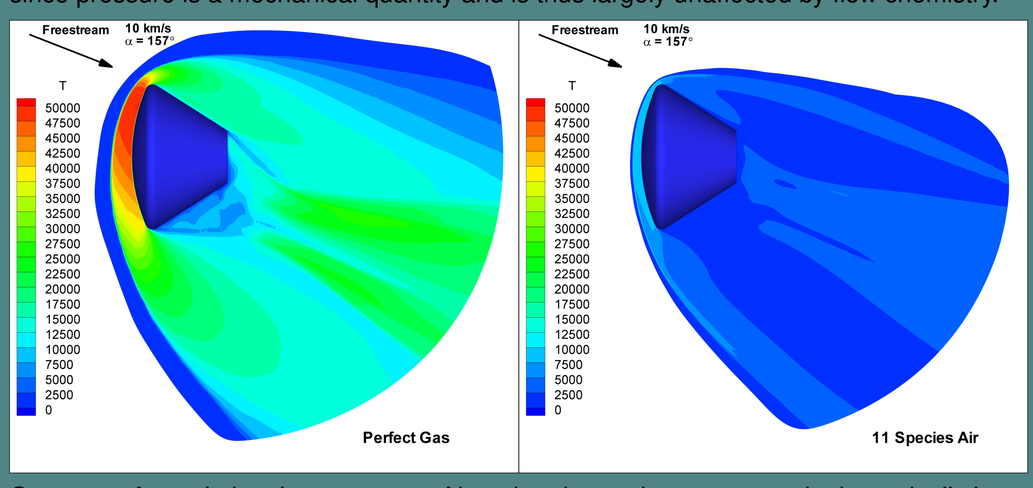

Contours of translational temperature. Note that the peak temperature is dramatically lower in the 11 species case. In the perfect gas case the kinetic energy of the flow is converted only to thermal energy because no chemical reactions are allowed. In the 11 species case much of the kinetic energy is used to dissociate and to a lesser extent to ionize the nitrogen and oxygen molecules present in the freestream air, and thus less energy goes into random thermal motion.

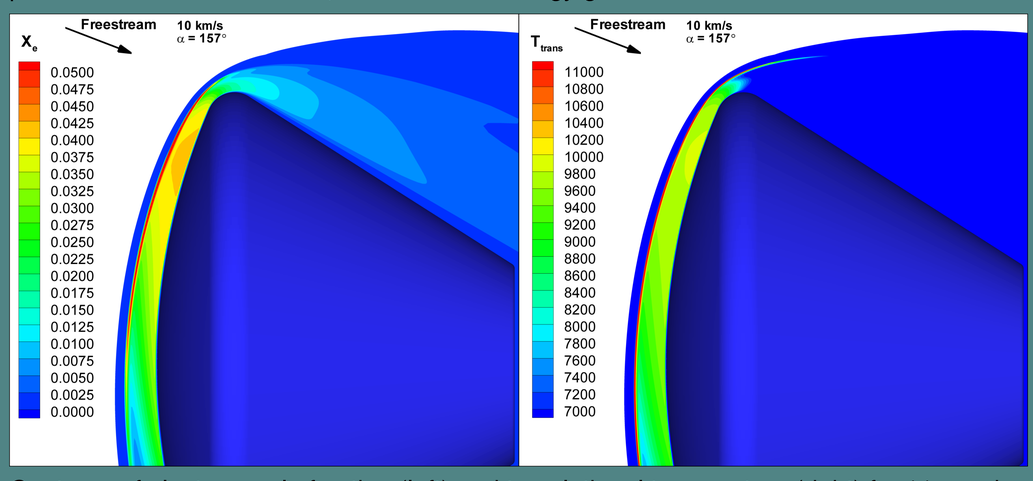

Contours of electron mole fraction (left) and translational temperature (right) for 11 species air. Since the plasma is quasi-neutral on scales greater than the Debye length, the mole fraction of electrons at any given point in the flowfield is approximately equal to the sum of the mole fractions of the positive ions. Thus the electron mole fraction is a reasonable measure of the degree of ionization. Degree of ionization is largest inside the bow shock. This high degree of ionization in the bow shock is explained by the fact that the electronic temperature in DPLR is set equal to the translational temperuture, and thus the ionization rate is highest where translational temperature is highest. Translational temperature, as expected, is highest inside the bow shock, before vibrational relaxation can occur. Thus, since ionization rate is linked to tranlational temperature, ionization is also highest inside and immediately behind the bow shock. Moving past the shock and closer to the body, ionization first decreases (due to vibrational relaxation and the corresponding drop in translational temperature) and then increases as the flow approaches the stagnation point and the translational temperature rises once again.

Surface Heat Transfer

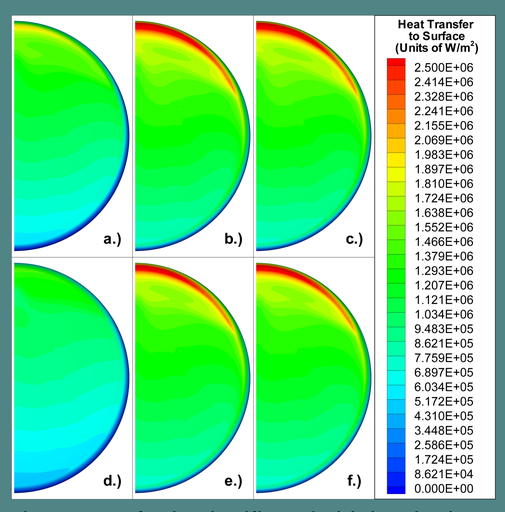

a.) Isothermal, non-catalytic wall.
b.) Isothermal, catalytic wall.
c.) Isothermal, supercatalytic wall.
d.) Radiative equilibrium, non-catalytic wall.
e.) Radiative equilibrium, catalytic wall.
f.) Radiative equilibrium, supercatalytic wall.

Contours of heat transfer to the surface of the heat shield. In the isothermal wall cases, the constant wall temperature was set to 1000K. In the radiative equilibrium cases the wall emissivity was set to 0.85. In the catalytic wall cases the catalytic efficiency was set equal to one and the wall was fully catalytic to ions.

The heat transfer is significantly higher in the catalytic and supercatalytic cases than in the non-catalytic case because the recombination reactions are exoergic. For each of the catalysis models, the heat transfer is found to be slightly lower in the radiative equilibrium case than in the isothermal wall case, because the surface temperatures in the radiative equilibrium cases are found to be higher than the 1000K isothermal wall temperature everywhere on the heat shield. Thus, the temperature gradient at the surface is lower and therefore the heat transfer due to conduction is lower.

Finally, the catalytic and supercatalytic cases are nearly identical, with very slightly lower heat transfer in the catalytic case. This agreement is a result of choosing a catalytic efficieny of one. The very slight difference comes from the fact that only the basic oxygen and nitrogen and ion-electron recombination reactions are included in the catalysis model. Any NO which is present at the wall is unaffected, and therefore some nitrogen and oxygen atoms remain locked in NO and are unavailable for recombination. In the supercatalytic wall case however, the species concentrations at the wall are simply set to their freestream values and the energy difference is transferred to the wall as heat. In the case of NO, the nitrogen and oxygen atoms are put back into molecular nitrogen and oxygen, respectively, and thus slightly more energy is transferred to the wall.